analytical chemistry

pubs.acs.org/ac Article

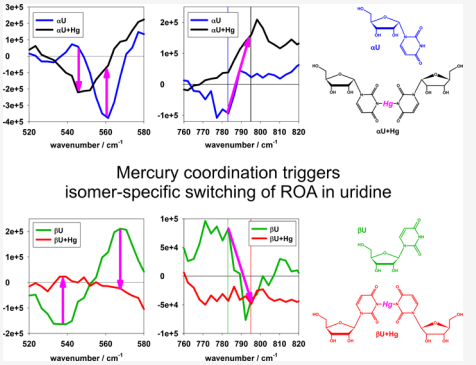
A Chiroptical Switch Owing to Mercury-Crosslinked Ribonucleosides

Vladimír Sychrovský,* Miloš Buděšínský,* Ivan Rosenberg,* Květoslava Kertisová, Ivana Kóšiová, Jiří Fukal, Yoshiyuki Tanaka, Debraj Gangopadhyay, and Petr Bouř

Cite This: *Anal. Chem.* 2026, 98, 26575−26582 Read Online

ACCESS | Metrics & More | Article Recommendations | Supporting Information

ABSTRACT: A highly specific chiroptical response of ribonucleoside diastereomers upon metallic crosslinking was demonstrated by Raman optical activity (ROA) spectroscopy. Three ROA diagnostic bands, assigned to prominent in-plane nucleobase ring deformations, undergo a concerted sign inversion upon mercury crosslinking. Virtually the same ROA sign switch was also observed upon a stereochemical modification (N1-glycosidic bond inversion) of a metal-free ribonucleoside. The prominent ROA sign switch thereby exemplified congruous chiroptical responses, owing to metal crosslinking and distinct ribonucleoside stereochemical modification. It is the first ROA detection of a metal-mediated base pair in mercury-crosslinked ribonucleosides evidenced by the ESI-MS and NMR measurements.



INTRODUCTION

Chiral systems respond differently to left- and right-circularly polarized light[1] and are typically studied by circular dichroism (CD) and optical rotation (OR) spectroscopies[2] as optical enantiomers (stereoisomers) generate antipodal (sign-inversion or mirror-imaged) spectra. To study diastereomers such as ribonucleosides investigated in the present study, the Raman optical activity (ROA) spectroscopy[3−5] is more appropriate because the vibrational assignment of Raman/ROA spectral bands facilitates identification of chiral center(s) in the molecule of interest. The ROA spectra we present here can indeed sense the individual diastereomers of the fundamental nucleic acid building blocks, upon crosslinking by mercury.

Nucleic acids and DNA polymers in general are well-suited as templates for making nanostructures with tailored optical properties.[6−8] Nucleic acids crosslinked by metal ions serving as coordination centers expand the nucleic acids' application range.[9−11] Metal-crosslinked base pairs such as T−Hg^{II}−T[12−14] and C−Ag^{I}−C[15] readily self-assemble, and other chemically modified nucleobases enable a wide range of metal−nucleic acid architectures.[16−18] Self-assembly, programmable polymer sequence, and tunable metal binding make it easy to transform these organometallic scaffolds to nanoscale molecular switches,[19,20] nanowires,[21−23] magnets,[24−26] rectifiers,[27] memory elements,[28] and sensing devices.[9,29−32]

The unique physicochemical properties of metalated nucleic acids underpin their application potential. Specific coordination of metals such as Cu^{II}, Hg^{II}, Ag^{I}, and $Au^{III/I}$ encountered in crystals[14,33−38] was confirmed in solution by NMR,[13,17,39−41] Raman,[39,42,43] surface-enhanced Raman (SERS)[44,45] and infrared (IR)[43] spectroscopy. Positive reaction entropy due to the formation of a metal-mediated base pair[46,47] via metal dehydration[48,49] exemplified "a solvent-shielded metallic chain inside organic polymer"[33,50]—a perfect analogue of a macroscopic metallic wire assembly that includes metal cations.

Canonical DNA has been eyed as a potential nanoelectronic material for decades[51] but the measured conductance properties varied widely, from insulating to superconducting.[27,52−56] Metal doping is anticipated to enhance conductance[57] and structural stability[58] of DNA, owing to unique (relativistic) properties of heavy metals. Recent reports on extended metallic arrays such as Ag−DNA chain[33] and Ag−DNA one-dimensional frameworks[34] exemplify that.

Chiral response to metalation[12,59,60] and effects due to inserting chiral metallic centers[61] make the organometallic polymers suitable as optoelectronic devices[62−65] and sensors.[66] In the present study, we introduce a chiroptical switch with a unique enantiospecific response, owing to mercury-crosslinked nucleic acid building blocks.

MATERIALS AND METHODS

Preparation and Spectral Analyses of Crosslinked Ribonucleosides

1-α-D-ribofuranosyluracil ($_{\alpha}$U) and 1-β-D-ribofuranosyluracil ($_{\beta}$U) nucleosides and mercury(II) acetate [$Hg^{II}(OAc)_2$] (Figure S1) were

Received: April 22, 2026
Revised: July 21, 2026
Accepted: August 10, 2026
Published: August 31, 2026



Downloaded from pubs.acs.org/anchem/article-pdf/98/36/26575/6797896/acs.analchem.6c02740.pdf by INST ORGANIC CHEMISTRY AND BIOCHEM user on 23 October 2026

© 2026 American Chemical Society

https://doi.org/10.1021/acs.analchem.6c02740
Anal. Chem. 2026, 98, 26575−26582

purchased from commercial suppliers. Note that chiro-specific detection of the $_{\alpha}$U and $_{\beta}$U diastereomers with ROA was due to the C1′ center (Figure S1).

Raman and ROA spectra for 0.225 ($_{\alpha}$U), 0.247 ($_{\beta}$U), and 1.059 M $Hg^{II}(OAc)_2$ stock solutions prepared in Milli-Q water were collected with the Zebr ROA spectrometer covering 50 to 4500 cm^{-1}; the laser power was 150−200 mW, and ROA spectra were accumulated for ∼24 h. Crosslinked nucleosides were obtained by mixing appropriate aliquots to achieve a 1:1 nucleoside-to-metal ratio. The response to an increasing mercury concentration was investigated for $_{\beta}$U (0.074 M) at Hg:$_{\beta}$U ratios of 1:5.6, 1:2.8, 1:1.9, and 1:1.4.

The ^{1}H and ^{13}C NMR spectra were recorded on a Bruker AVANCE-600 spectrometer (^{1}H at 600.13 MHz, ^{13}C at 150.9 MHz) in D_2O or DMSO-d_6 solution. The 2D-^{1}H, ^{1}H−COSY, 2D-^{1}H, ^{13}C-HSQC and 2D-^{1}H, ^{13}C-HMBC spectra were used for the structural assignment of proton and carbon signals. The ^{15}N chemical shifts were obtained from 2D-^{15}N, ^{1}H-HMBC spectra recorded on the same instrument. ^{199}Hg NMR spectrum of the $_{\beta}U-^{199}Hg^{II}-_{\beta}U$ complex was recorded using $^{15}N3$-labeled $_{\beta}$U (4.7 mg) in DMSO-d_6 (0.5 mL) on a JEOL ECZR-500 spectrometer at 89.42 MHz. Mercury-crosslinked nucleosides were prepared by adding $Hg^{II}(OAc)_2$ to uridine solution in D_2O or DMSO-d_6 at the desired molar ratio, typically with a slight excess of mercury acetate.

High-resolution ESI-MS spectra were measured using LTQ Orbitrap XL (Thermo Fisher Scientific) for the $_{\beta}U-Hg^{II}-_{\beta}U$ complex in DMSO-d_6 applied by direct injection in positive mode and 80% MeOH mobile phase.

Density functional theory (DFT) calculations were performed using the B3LYP functional[67−70] with the CPCM model for water solvent,[71,72] "very tight" SCF criteria, and an ultrafine (199 974-point) integration grid, as implemented in Gaussian 09 (revision E.01).[73] Geometry optimizations and Raman/ROA spectra were computed with the 6−311+G(2d,p) basis[74] for light atoms, and the Stuttgart RSC ECP basis[75] for Hg. NMR chemical shifts were calculated using the IGLO-III basis[76] within the GIAO approach[77−81] while referencing to the metal-free nucleoside. Assignment of Raman bands was aided by GaussView 6.016 and our software.

RESULTS

Primary Detection of the Metallic Crosslink

The mercury-crosslinked uridine pair was first measured by ESI-MS. The calculated monoisotopic mass of $C_{18}H_{22}HgN_4O_{12}$ $[M + Na]^+$ ($_{\beta}U-^{202}Hg^{II}-_{\beta}U$) was 711.08327 Da. This matched the measured mass of 711.08390 Da, with a scatter due to the naturally present mercury isotopes (Figure 1). The 708.08148 Da peak corresponds to the ^{199}Hg isotope and relevant $_{\beta}U-^{199}Hg^{II}-_{\beta}U$ complex was NMR-detected as described below.

We used $^{15}N3$-labeled $_{\beta}$U to detect a mercury-crosslinked uridine dimer by NMR, following the $T-Hg^{II}-T$ base pair identification by Dairaku et al.[40] Splitting of the ^{199}Hg resonance (Figure 2A) confirmed the formation of $_{\beta}U-Hg^{II}-_{\beta}U$ complex, and the triplet at −1772 ppm with $^{1}J(^{199}Hg, ^{15}N3)$ = 1026.8 Hz evidenced the $(_{\beta}U)N3-Hg^{II}-N3(_{\beta}U)$ linkage (Figure 2D).

Metal-induced ^{15}N and ^{13}C chemical shifts indicative of an identical Hg^{II} coordination for $_{\alpha}$U (Figure 2B, C) and $_{\beta}$U (Figure 2D, E) in both DMSO and D_2O are consistent with other NMR studies of similar complexes.[13,82] The downfield N3 shift (∼30 ppm) and progressive attenuation of the induced shifts through adjacent carbonyl carbons (∼3 ppm) and ring carbons (<1 ppm) are in agreement with calculated data (Figure S4). Ribose shifts below 1 ppm confirmed that the nucleobase served as the metal-binding site. The visible similarity of the metal-induced chemical shifts confirmed analogous crosslinking for $_{\alpha}$U and $_{\beta}$U isomers (Figure 2).

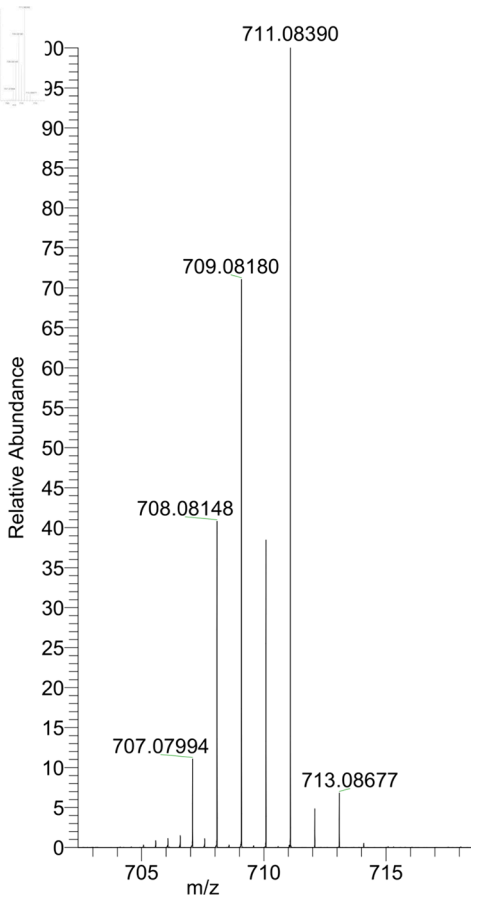


Figure 1. Electrospray-ionization mass spectrum (ESI-MS) of $C_{18}H_{22}HgN_4O_{12}$ $[M + Na]^+$. A spectrum of $C_{18}H_{22}HgN_4O_{12}$ $[M + H]^+$ is shown in Figure S3.

Raman Detection of the Crosslinked Ribonucleosides Is Isomer-Insensitive

Raman-band assignment (Table 1, Figure 3) was guided by DFT analysis and published data for metal-free uridine crystals.[83] Prominent spectral features between 1680 and 1625 cm^{-1} correspond to the C=O and C5=C6 stretching vibrations. Upon metalation, these bands shifted from 1678/1680 cm^{-1} ($_{\alpha}U/_{\beta}U$) to 1639/1582 cm^{-1} ($_{\alpha}U + Hg$) and 1642/1579 cm^{-1} ($_{\beta}U + Hg$), reflecting symmetric and antisymmetric C=O stretching of the U-ring carbonyls. Additional shifts of the C5=C6/C=O bands from 1625/1630 to 1669/1675 cm^{-1} confirmed a perturbation of the π-system by metal coordination.

Bands between 1473 and 998 cm^{-1} were assigned to the U-ring stretching and N3−Hg-related wagging/scissoring modes. Metalation induced noticeable shifts from −18 to +54 cm^{-1}, with new bands at 1290 and 1090 cm^{-1} due to coupled C6−H6/N3−Hg vibrations. The prominent 1233 cm^{-1} band exhibited a small upshift (+5 cm^{-1}), while the ∼1000 cm^{-1} band (asymmetric U-ring stretching and C1′−C2′ stretching) shifted by +54 cm^{-1}, which is consistent with the N3−Hg wagging.

Raman bands in the 867−420 cm^{-1} region reflected deformations of the nucleobase and ribose, scissoring of the exoring groups and N3−Hg stretching vibrations. The 783 cm^{-1} band, assigned to the symmetric U-ring breathing, shifted by +12 cm^{-1} upon adding Hg. This corresponds to symmetric vibrational coupling within the $N3-Hg^{II}-N3$ linkage, and

Downloaded from pubs.acs.org/anchem/article-pdf/98/36/26575/6797896/acs.analchem.6c02740.pdf by INST ORGANIC CHEMISTRY AND BIOCHEM user on 23 October 2026

https://doi.org/10.1021/acs.analchem.6c02740
Anal. Chem. 2026, 98, 26575−26582

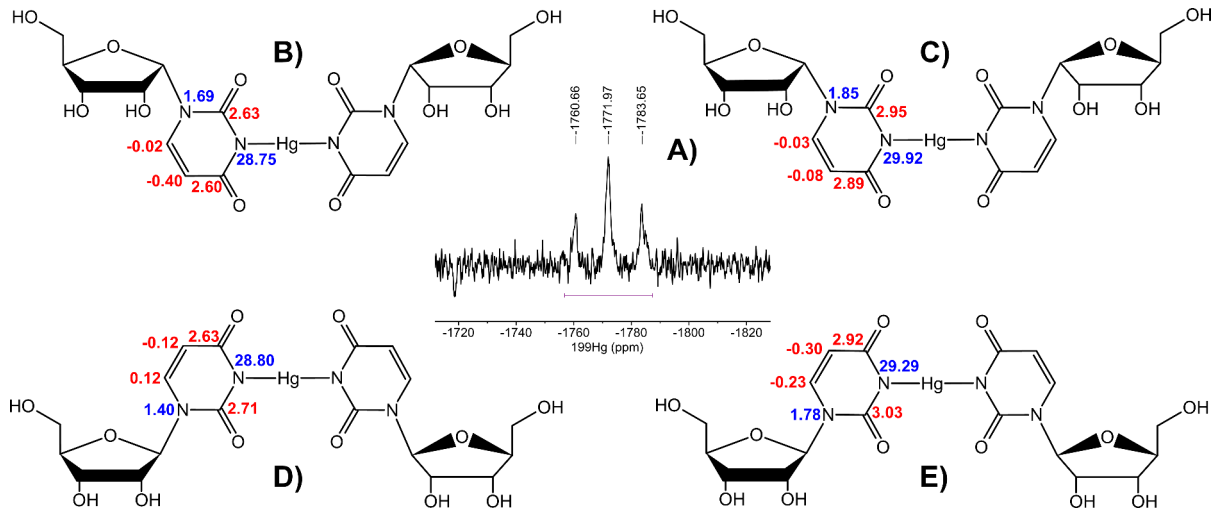


Figure 2. ^{199}Hg NMR spectrum demonstrating the indirect spin−spin coupling $^{1}J(^{199}\mathrm{Hg}, ^{15}\mathrm{N3})$ 1026.8 Hz for $_{\beta}$U in DMSO-d_6 upon adding mercury (A), and metal-induced ^{13}C/^{15}N NMR shifts (colored red/blue) in $_{\alpha}$U in DMSO-d_6 (B) and D_2O (C), and $_{\beta}$U in DMSO-d_6 (D) and D_2O (E).

Table 1. Assignments of Raman Bands (cm^{-1}) for $_{\alpha}$U, $_{\beta}$U and Hg-Crosslinked Nucleosides[a]

$_{\alpha}$U	$_{\beta}$U	$_{\alpha}$U +Hg	$_{\beta}$U +Hg	Assignment
1678[b]	1680[b]	1639	1642	ν(C=O) (*s*), ν(C5=C6)
1678[b]	1680[b]	1582	1579	*m*: ν(C=O) (*as*), ν(C5=C6), *d*: ν(C=O) (*as*)
1625	1630	1669	1675	*m*: ν(C5=C6), ν(C=O), *d*: ν(C5=C6), ν(C2=O)
1476	1473	1458	1455	ν(U-Ring) (as), *wg*(H1′)
1404	1398	1393	1388	ν(N3−C2/C4) (*s*), ν(C5−C4/C6) (*s*), ν(C2−N1/N3 (*as*), ν(N3−Hg)
n.d.	n.d.	1292	1290	ν(N1−C2/C6) (*as*), ν(N3−C2/C4) (*as*), *wg*(C6−H6), *wg*(N3−Hg)
1233	1233	1241	1238	ν(N1−C2/C6) (*as*), ν(N3−C2/C4 (*as*), *wg*(C5−H5), *wg*(N3−Hg)
1123	1134	1120	1125	ν(N1−C2) (*s*), ν(N3−C4) (*s*), *sc*(C5/C6−H), ν(N1−C1′), ν(N3−Hg)
n.d.	n.d.	1092	1089	ν(N1−C2, N3−C4) (*s*), *sc*(C5/C6−H), ν(C2′-O), ν(N3−Hg)
1001	998	1055	1052	ν(N1−C2, C4−C5) (*as*), ν(C1′-C2′), *wg*(N3−Hg)
864	867	867, 896	867, 896	U-Ring breathing, R-ring out-of-plane, ν(C1′-N1), ν(N3−Hg)
783	783	795	795	Centre-symmetric in-plane U-ring breathing, ν(N3−Hg) (*s*)
720	720	729	735	R-ring deform, ν(C1′−N1), ν(N1−C2)
n.d.	n.d.	701	698	U-ring in-plane twisting, ν(N3−Hg)
561	564	561	568	U-ring in-plane stretching along C2−C5 direction, ν(N3−Hg) (*s*), R-ring breathing
558	555	605	605	U-ring in-plane stretching along C2−C5 direction, ν(N3−Hg) (*as*)
542	532	547	539	U-ring in-plane stretching along N1−C4 direction, ν(C4=O, C5−H) (*sc*), R-ring deformation along C2′−C4′, ν + *wg*(N3−Hg)
427	420	459	459	ν(C=O) (*sc*), ν(N3−Hg) (*s*)

[a]A full dataset may be found in Table S1. [b]Broad band including two bands indicated by DFT calculations (Table S1). $_{\alpha}$U, 1-α-D-ribofuranosyluracil. $_{\beta}$U, 1-β-D-ribofuranosyluracil. **m**, metal-free nucleoside. **d**, metal-crosslinked nucleosides. **R**, ribose. **ν**, stretching vibration. **s**, symmetric vibration. **as**, antisymmetric vibration. **sc**, scissoring vibration. **wg**, wagging vibration. **n.d.**, not detected.

agrees with the study by Mansy and Tobias.[84] In uridine crystals, this U-ring breathing band ranged from 779 to 789 cm^{-1}.[83] New spectral features around 700 cm^{-1} indicated N3−Hg stretching coupled with U-ring twisting. The broad 867 cm^{-1} band (DFT calculation indicated two bands, Table S1) appears to have split upon metalation, yielding a new, stronger band at 893 cm^{-1}.

Bands between 568 and 420 cm^{-1} were assigned to in-plane U-ring deformations, exogroup scissoring, and N3−Hg stretching. The ∼560 cm^{-1} band due to U-ring stretching in the C2−C5 direction remained largely unchanged. A +50 cm^{-1} upshift of the ∼555 cm^{-1} band indicated asymmetric N3−Hg^{II}−N3 stretching. The 542/532 cm^{-1} band (of $_{\alpha}$U/$_{\beta}$U) due to the U-ring stretching in the N1−C4 direction shifted up to a tiny bit, and included the N3−Hg stretching/wagging. The ∼420 cm^{-1} band (carbonyl scissoring) shifted up by ca. +30 cm^{-1} due to the symmetric N3−Hg stretching.

Overall, the data document the metal-crosslink formation consistently with the NMR data. The Raman spectra alone, however, could not distinguish between $_{\alpha}$U and $_{\beta}$U crosslinked forms, thus prompting further investigation by a more appropriate ROA spectroscopy.

Isomer-Specific Detection of Metal Crosslinked Nucleosides by ROA

Most of chiroptical ROA bands (Figure 3) have not changed upon Hg crosslinking, and only several exhibited shifts consistent with the corresponding Raman bands. For example, the 1400, 1230, and 870 cm^{-1} bands (stretching of the N1-glycosidic bond and adjacent atomistic motions) were strongly isomer-dependent, and thus enable isomer identification/detection. Only three ROA bands exhibited a distinct sign inversion ("switch") upon metalation, thus providing an unambiguous diagnostic signature of the crosslink formation.

The ROA patterns of metal-free $_{\alpha}$U and $_{\beta}$U nucleosides mostly feature opposite signs between 520 and 600 cm^{-1} (Figure 4A). In $_{\alpha}$U, upon addition of mercury, the 542 and 558 cm^{-1} bands switched sign from "+ −" to "− +" (Figure 4B), and the opposite was the case in $_{\beta}$U (Figure 4C). The corresponding vibrations involve prominent in-plane deformations of U-ring in the N1−C4 or C2−C5 direction plus N3−Hg stretching (Table 1). A stepwise ROA sign inversion

https://doi.org/10.1021/acs.analchem.6c02740
Anal. Chem. 2026, 98, 26575−26582

Downloaded from pubs.acs.org/anchan/article-pdf/98/36/26575/6797296/acs.analchem.6c02740.pdf by INST ORGANIC CHEMISTRY AND BIOCHEM user on 23 October 2026

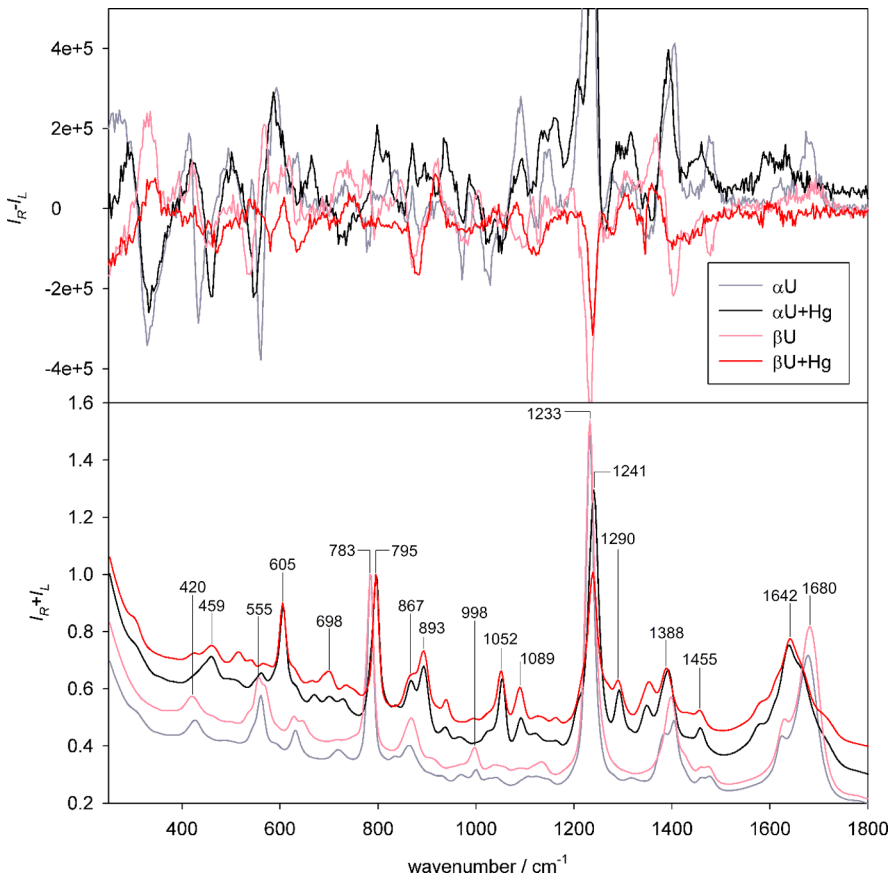


Figure 3. ROA (I_R−I_L) and Raman (I_R+I_L) spectra of metal-free and Hg-crosslinked $_{\alpha}$U and $_{\beta}$U nucleosides. Raman spectra are normalized relative to the U-ring breathing band (783 respective 795 cm^{-1}). Raman spectra (as measured) and ROA spectra scaled by measured Raman intensities are shown in Figure S5.

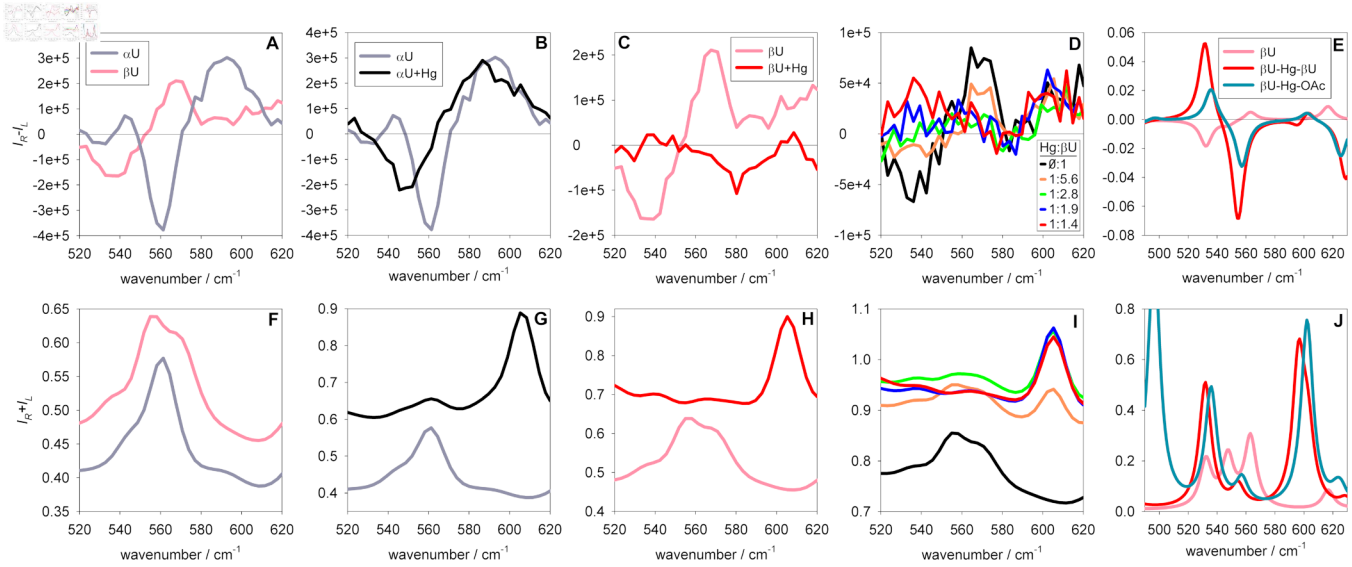


Figure 4. ROA (I_R−I_L) and Raman (I_R+I_L) bands in the spectral-switch region. (A, F) Metal-free. (B, G) Hg-crosslinked $_{\alpha}$U. (C, H) Hg-crosslinked $_{\beta}$U. (D, I) $_{\beta}$U upon gradual mercury adding. (E, J) DFT-calculated bands for $_{\beta}$U nucleoside and $_{\beta}$U−Hg^{II}−OAc and $_{\beta}$U−Hg^{II}− $_{\beta}$U complexes. Raman spectra are normalized relative to the U-ring breathing band (783 respective 795 cm^{-1}).

induced upon gradual addition of mercury (Figure 4D, Table S2) confirmed the chiroptical response to metal crosslinking.

An additional ROA signal inversion was encountered for the symmetric U-ring breathing mode, which shifted from 783 to 795 cm^{-1} upon Hg-crosslinking. Again, $_{\alpha}$U exhibited a "−" ROA pattern at 783 cm^{-1}, while $_{\beta}$U showed antipodal "+" pattern (Figure 5A). Upon adding Hg, the ROA signal of $_{\alpha}$U switched to a "+" pattern at 795 cm^{-1} (Figure 5B), and conversely, the ROA signal of $_{\beta}$U switched to a "−" pattern (Figure 5C). Sign inversion of the ROA band in $_{\beta}$U progressed

https://doi.org/10.1021/acs.analchem.6c02740
Anal. Chem. 2026, 98, 26575−26582

Downloaded from pubs.acs.org/anchem/article-pdf/98/36/26575/6797896/acs.analchem.6c02740.pdf by INST ORGANIC CHEMISTRY AND BIOCHEM user on 23 October 2026

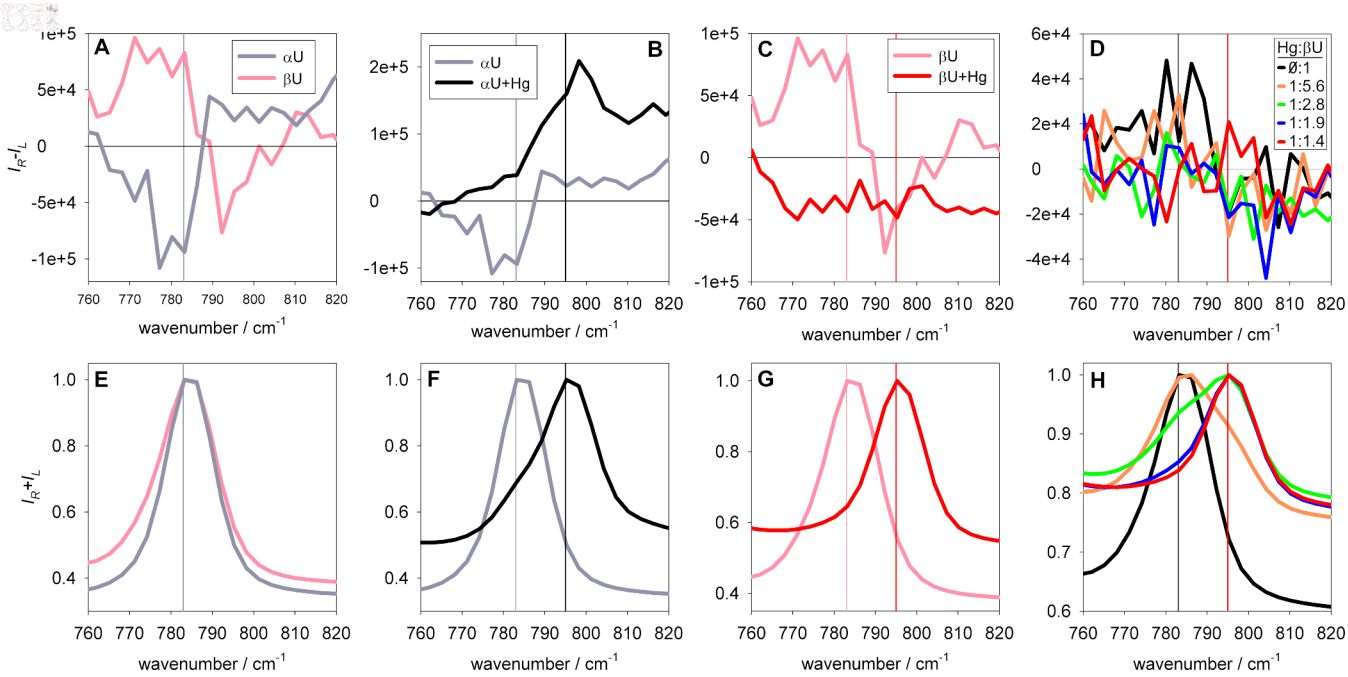


Figure 5. ROA (I_R-I_L) and Raman (I_R+I_L) bands for ring breathing in the spectral-switch region. (A, E) metal-free nucleosides. (B, F) Hg-crosslinked $_{\alpha}$U. (C, G) Hg-crosslinked $_{\beta}$U. (D, H) $_{\beta}$U upon gradual mercury adding. Raman spectra normalized relative to U-ring breathing.

stepwise with increasing Hg concentration (Figure 5D, Table S2).

Chiroptical response of the three ROA diagnostic bands to N-glycosidic bond inversion was more pronounced than their response to metalation. Nevertheless, the effect due to distinct chiral inversion at the C1′ center was "reversed" upon binding of virtually achiral metal center, indicating thus unique capability of the heavy metal.

DISCUSSION

Summary of Spectral Findings

The spectroscopic analyses establish that formation of the (U)N3−Hg^{II}−N3(U) crosslink leads to a distinct, isomer-dependent inversion ("switch") of the vibrational ROA bands associated with the prominent in-plane deformations of the uracil ring. In contrast, the conventional Raman bands are isomer-insensitive. An excess of mercury could affect Raman (Figures S6 and S7, Table S3) but not ROA spectra (Figure S8). The ROA switch, manifested as a concerted sign reversal of the three fingerprint bands, thus constitutes a reliable, isomer-specific spectroscopic hallmark of a metal-crosslinked nucleosides.

Theoretical Analysis of ROA Switch

The DFT-optimized geometries (Figure S2) revealed a substantial twisting of the Hg-linked $_{\beta}$U nucleobases (~90°), exceeding the ~30° twist observed in the T−Hg^{II}−T crystal structure (PDB ID 4L24).[14] Such an orthogonal twist of the U rings generates a nearly perpendicular orientation of the transition electric dipoles contributing to the polarizabilities involved in the in-plane vibrations (ROA switch). Indeed, calculation of the ROA spectra using the electric−dipole−electric−dipole polarizability term only[85] indicated this component as dominant (Figure S9).

The observed ROA-signal switching may thus arise from a coupling of group polarizabilities within the Hg-crosslinked moieties. Nevertheless, the DFT simulations for $_{\beta}$U, $_{\beta}$U−Hg^{II}−OAc (heterocomplex), and $_{\beta}$U−Hg^{II}−$_{\beta}$U (homodimer) (Figure 4E) demonstrated that the ROA switching pattern originates directly from Hg coordination at the nucleobase where it perturbs the local electronic environment and, hence, the optical response of the in-plane U ring vibrations, leading to the ROA sign flip (Figure 4E).

The DFT calculations elucidated the effect in detail. Upon metalation, the 548 cm^{-1} band exhibited a + 50 cm^{-1} upshift to outside the ROA switching region (Figure 4J), and the sign inversion of the 532 and 563 cm^{-1} bands (Figure 4E) matched the experimental data (Figure 4C). The ROA pattern computed for the $_{\beta}$U−Hg^{II}−OAc heterocomplex (Figure 4E) indicates that the ROA-switching pattern is driven purely by coordination of mercury to the nucleobase.

CONCLUSIONS

Raman optical activity spectroscopy of the uridine diastereomers revealed a distinct isomer-specific chiroptical response due to mercury crosslinking. The metallic linkage, confirmed independently by the ESI-MS and NMR measurements, brought about an inversion (sign flip or "switch") of the prominent ROA signature bands due to the uracil ring deformations. This constitutes an isomer-specific chiroptical marker of metal-mediated base pair formation.

Virtually the same ROA signature, as exemplified upon metal uptake, was observed due to the N1-glycosidic bond inversion in the metal-free nucleoside. The ROA spectroscopy thereby exemplified chiroptical responses of uridine due to the metal linkage and stereochemical configuration change of prominent center, such as the anomeric C1′ carbon in the ribonucleoside.

This newly identified chiroptical signature extends the analytical scope of ROA spectroscopy to metalloorganic scaffolds and paves the way for advanced chiroptical sensing.

https://doi.org/10.1021/acs.analchem.6c02740
Anal. Chem. 2026, 98, 26575−26582

Downloaded from pubs.acs.org/anchem/article-pdf/98/36/26575/6797896/acs.analchem.6c02740.pdf by INST ORGANIC CHEMISTRY AND BIOCHEM user on 23 October 2026

■ ASSOCIATED CONTENT

Supporting Information

The Supporting Information is available free of charge at https://pubs.acs.org/doi/10.1021/acs.analchem.6c02740.

Chemical structures of studied complexes, ESI-MS spectrum, calculated NMR shifts, raw Raman/ROA spectra of analyzed compounds, refined and calculated spectrum for mercury acetate and additional tables of vibrations (PDF)

■ AUTHOR INFORMATION

Corresponding Authors

Vladimír Sychrovský − *Institute of Organic Chemistry and Biochemistry, Czech Academy of Sciences, Praha 16000, Czech Republic*; Email: vladimir.sychrovsky@uochb.cas.cz

Miloš Buděšínský − *Institute of Organic Chemistry and Biochemistry, Czech Academy of Sciences, Praha 16000, Czech Republic*; Email: milos.budesinsky@uochb.cas.cz

Ivan Rosenberg − *Institute of Organic Chemistry and Biochemistry, Czech Academy of Sciences, Praha 16000, Czech Republic*; orcid.org/0000-0003-0921-9597; Email: ivan.rosenberg@uochb.cas.cz

Authors

Květoslava Kertisová − *Institute of Organic Chemistry and Biochemistry, Czech Academy of Sciences, Praha 16000, Czech Republic*

Ivana Kóšiová − *Institute of Organic Chemistry and Biochemistry, Czech Academy of Sciences, Praha 16000, Czech Republic*

Jiří Fukal − *Institute of Organic Chemistry and Biochemistry, Czech Academy of Sciences, Praha 16000, Czech Republic; Department of Physical Chemistry, Palacký University Olomouc Faculty of Science, Olomouc 77146, Czech Republic*

Yoshiyuki Tanaka − *Laboratory of Analytical Chemistry, Tokushima Bunri University Faculty of Pharmaceutical Sciences, Yamashiro-cho, Tokushima 770-8514, Japan*; orcid.org/0000-0001-9703-2014

Debraj Gangopadhyay − *Institute of Organic Chemistry and Biochemistry, Czech Academy of Sciences, Praha 16000, Czech Republic*; orcid.org/0000-0002-5249-3041

Petr Bouř − *Institute of Organic Chemistry and Biochemistry, Czech Academy of Sciences, Praha 16000, Czech Republic*

Complete contact information is available at: https://pubs.acs.org/10.1021/acs.analchem.6c02740

Author Contributions

Project administration: **V.S.** Conceptualization: **V.S., M.B., I.R.** Methodology: **V.S., M.B., K.K., I.K., J.F., P.B.** Investigation: **V.S., M.B., K.K., J.F., P.B.** Formal analysis: **D.G., P.B.** Visualization: **M.B., K.K., J.F.** Supervision: **V.S., M.B., I.R., Y.T.** Writing−original draft: **V.S.** Writing−review and editing: **V.S., M.B., D.G., P.B.** Funding acquisition: **I.R., P.B.**

Funding

Czech Science Foundation GAČR, Grant No. 25−15726S, Ministry of Education.

Notes

The authors declare no competing financial interest.

■ ACKNOWLEDGMENTS

Computational resources were provided by the e-INFRA CZ project (ID:90254), supported by the Ministry of Education, Youth and Sports of the Czech Republic.

■ ABBREVIATIONS

ROA, Raman Optical Activity; CD, circular dichroism; OR, optical rotation; SERS, surface-enhanced Raman spectroscopy; IR, infrared; DMSO-d_6, deuterated dimethyl sulfoxide; $_{\alpha}$U, 1-α-D-ribofuranosyluracil; $_{\beta}$U, 1-β-D-ribofuranosyluracil; $Hg^{II}(OAc)_2$, mercury(II) acetate

■ REFERENCES

(1) Barron, L. D. *Molecular Light Scattering and Optical Activity*; Cambridge University Press, 2004.

(2) Yoo, S.; Park, Q. H. Metamaterials and chiral sensing: a review of fundamentals and applications. *Nanophotonics−Berlin* **2018**, *8* (2), 249−261.

(3) Profant, V.; Jílek, S. Transformative progress in Raman optical activity: recent advances and innovations. *Appl. Spectrosc Rev.* **2026**, *61*, 1−37.

(4) Parchaňský, V.; Kapitán, J.; Bouř, P. Inspecting chiral molecules by Raman optical activity spectroscopy. *RSC Adv.* **2014**, *4* (100), 57125−57136.

(5) Nafie, L. A. Infrared and Raman vibrational optical activity: Theoretical and experimental aspects. *Annu. Rev. Phys. Chem.* **1997**, *48*, 357−386.

(6) Kuzyk, A.; Schreiber, R.; Fan, Z. Y.; Pardatscher, G.; Roller, E. M.; Högele, A.; Simmel, F. C.; Govorov, A. O.; Liedl, T. DNA-based self-assembly of chiral plasmonic nanostructures with tailored optical response. *Nature* **2012**, *483* (7389), 311−314.

(7) Martens, K.; Binkowski, F.; Nguyen, L.; Hu, L.; Govorov, A. O.; Burger, S.; Liedl, T. Long- and short-ranged chiral interactions in DNA-assembled plasmonic chains. *Nat. Commun.* **2021**, *12* (1), 1−6.

(8) Martynenko, I. V.; Erber, E.; Ruider, V.; Dass, M.; Posnjak, G.; Yin, X.; Altpeter, P.; Liedl, T. Site-directed placement of three-dimensional DNA origami. *Nat. Nanotechnol* **2023**, *18* (12), 1456−1462.

(9) Tanaka, Y.; Kondo, J.; Sychrovský, V.; Šebera, J.; Dairaku, T.; Saneyoshi, H.; Urata, H.; Torigoe, H.; Ono, A. Structures, physicochemical properties, and applications of T-Hg-T, C-Ag-C, and other metallo-base-pairs. *Chem. Commun.* **2015**, *51* (98), 17343−17360.

(10) Jash, B.; Müller, J. Metal-Mediated Base Pairs: From Characterization to Application. *Chem.—Eur. J.* **2017**, *23* (68), 17166−17178.

(11) Naskar, S.; Guha, R.; Müller, J. Metal-Modified Nucleic Acids: Metal-Mediated Base Pairs, Triples, and Tetrads. *Angew. Chem. Int. Edit* **2020**, *59* (4), 1397−1406.

(12) Miyake, Y.; Togashi, H.; Tashiro, M.; Yamaguchi, H.; Oda, S.; Kudo, M.; Tanaka, Y.; Kondo, Y.; Sawa, R.; Fujimoto, T.; et al. Mercury-mediated formation of thymine-Hg-thymine base pairs in DNA duplexes. *J. Am. Chem. Soc.* **2006**, *128* (7), 2172−2173.

(13) Tanaka, Y.; Oda, S.; Yamaguchi, H.; Kondo, Y.; Kojima, C.; Ono, A. ^{15}N-^{15}N J-coupling across Hg^{II} Direct observation of Hg-mediated T-T base pairs in a DNA duplex. *J. Am. Chem. Soc.* **2007**, *129* (2), 244−245.

(14) Kondo, J.; Yamada, T.; Hirose, C.; Okamoto, I.; Tanaka, Y.; Ono, A. Crystal Structure of Metallo DNA Duplex Containing Consecutive Watson-Crick-like T-Hg-T Base Pairs. *Angew. Chem. Int. Edit* **2014**, *53* (9), 2385−2388.

(15) Ono, A.; Cao, S.; Togashi, H.; Tashiro, M.; Fujimoto, T.; Machinami, T.; Oda, S.; Miyake, Y.; Okamoto, I.; Tanaka, Y. Specific interactions between silver(I) ions and cytosine-cytosine pairs in DNA duplexes. *Chem. Commun.* **2008**, *44* (39), 4825−4827.

Downloaded from pubs.acs.org/anchem/article-pdf/98/36/26575/6797296/acs.analchem.6c02740.pdf by INST ORGANIC CHEMISTRY AND BIOCHEM user on 23 October 2026

(16) Yang, H.; McLaughlin, C. K.; Aldaye, F. A.; Hamblin, G. D.; Rys, A. Z.; Rouiller, I.; Sleiman, H. F. Metal-nucleic acid cages. *Nat. Chem.* **2009**, *1* (5), 390−396.
(17) Johannsen, S.; Megger, N.; Böhme, D.; Sigel, R. K. O.; Müller, J. Solution structure of a DNA double helix with consecutive metal-mediated base pairs. *Nat. Chem.* **2010**, *2* (3), 229−234.
(18) Takezawa, Y.; Müller, J.; Shionoya, M. Artificial DNA Base Pairing Mediated by Diverse Metal Ions. *Chem. Lett.* **2017**, *46* (5), 622−633.
(19) Schmidt, O. P.; Jurt, S.; Johannsen, S.; Karimi, A.; Sigel, R. K. O.; Luedtke, N. W. Concerted dynamics of metallo-base pairs in an A/B-form helical transition. *Nat. Commun.* **2019**, *10*, 1−11.
(20) Artés, J. M.; Li, Y. H.; Qi, J. Q.; Anantram, M. P.; Hihath, J. Conformational gating of DNA conductance. *Nat. Commun.* **2015**, *6*, 1−8.
(21) Isobe, H.; Yamazaki, N.; Asano, A.; Fujino, T.; Nakanishi, W.; Seki, S. Electron Mobility in a Mercury-mediated Duplex of Triazole-linked DNA (^{TL}DNA). *Chem. Lett.* **2011**, *40* (3), 318−319.
(22) Liu, S.; Clever, G. H.; Takezawa, Y.; Kaneko, M.; Tanaka, K.; Guo, X. F.; Shionoya, M. Direct Conductance Measurement of Individual Metallo-DNA Duplexes within Single-Molecule Break Junctions. *Angew. Chem. Int. Edit* **2011**, *50* (38), 8886−8890.
(23) Ono, A.; Kanazawa, H.; Ito, H.; Goto, M.; Nakamura, K.; Saneyoshi, H.; Kondo, J. Novel DNA Helical Wire Containing Hg-Mediated T:T and T:G Pairs. *Angew. Chem. Int. Edit* **2019**, *58* (47), 16835−16838.
(24) Tanaka, K.; Tengeiji, A.; Kato, T.; Toyama, N.; Shionoya, M. A discrete self-assembled metal array in artificial DNA. *Science* **2003**, *299* (5610), 1212−1213.
(25) Mallajosyula, S. S.; Pati, S. K. Conformational Tuning of Magnetic Interactions in Metal-DNA Complexes. *Angew. Chem. Int. Edit* **2009**, *48* (27), 4977−4981.
(26) Clever, G. H.; Reitmeier, S. J.; Carell, T.; Schiemann, O. Antiferromagnetic Coupling of Stacked Cu^{II}-Salen Complexes in DNA. *Angew. Chem. Int. Edit* **2010**, *49* (29), 4927−4929.
(27) Kékedy-Nagy, L.; Ferapontova, E. E. Directional Preference of DNA-Mediated Electron Transfer in Gold-Tethered DNA Duplexes: Is DNA a Molecular Rectifier? *Angew. Chem. Int. Edit* **2019**, *58* (10), 3048−3052.
(28) De, A.; Lu, B. D.; Ohayon, Y. P.; Woloszyn, K.; Livernois, W.; Perren, L.; Yang, C. F.; Mao, C. D.; Botana, A. S.; Hihath, J.; et al. Transmetalation for DNA-Based Molecular Electronics. *Small* **2025**, *21* (25), 2411518.
(29) Ono, A.; Togashi, H. Highly selective oligonucleotide-based sensor for mercury(II) in aqueous solutions. *Angew. Chem. Int. Edit* **2004**, *43* (33), 4300−4302.
(30) Han, D.; Lim, S. Y.; Kim, B. J.; Piao, L.; Chung, T. D. Mercury(II) detection by SERS based on a single gold microshell. *Chem. Commun.* **2010**, *46* (30), 5587−5589.
(31) Li, Y. P.; Yang, Y. Q.; Zhong, C. M.; Xiao, D.; Zhou, C. S. Highly Sensitive Detection of T790 M with a Three-Level Characteristic Current by Thymine-Hg(II)-Thymine in the α-Hemolysin Nanopore. *Anal. Chem.* **2024**, *96* (8), 3587−3592.
(32) Kotammagari, T. K.; Al-Waeel, M.; Lukkari, J.; Lönnberg, T. Organomercury oligonucleotide-polydopamine nanoparticle assemblies discriminate between target sequences by Hg^{II}-mediated base pairing. *RSC Adv.* **2024**, *14* (51), 38279−38284.
(33) Kondo, J.; Tada, Y.; Dairaku, T.; Hattori, Y.; Saneyoshi, H.; Ono, A.; Tanaka, Y. A metallo-DNA nanowire with uninterrupted one-dimensional silver array. *Nat. Chem.* **2017**, *9* (10), 956−960.
(34) Atsugi, T.; Ono, A.; Tasaka, M.; Eguchi, N.; Fujiwara, S.; Kondo, J. A Novel Ag^{I}-DNA Rod Comprising a One-Dimensional Array of 11 Silver Ions within a Double Helical Structure. *Angew. Chem. Int. Ed.* **2022**, *61* (31), e202204798.
(35) Kosturko, L. D.; Folzer, C.; Stewart, R. F. Crystal and Molecular-Structure of a 2−1 Complex of 1-Methylthymine-Mercury-(Ii). *Biochemistry-Us* **1974**, *13* (19), 3949−3952.
(36) Atwell, S.; Meggers, E.; Spraggon, G.; Schultz, P. G. Structure of a copper-mediated base pair in DNA. *J. Am. Chem. Soc.* **2001**, *123* (49), 12364−12367.
(37) Ennifar, E.; Walter, P.; Dumas, P. A crystallographic study of the binding of 13 metal ions to two related RNA duplexes. *Nucleic Acids Res.* **2003**, *31* (10), 2671−2682.
(38) Kosugi, K.; Sugawara, A.; Iwase, E.; Park, H.; Fujiwara, S.; Kanazawa, H.; Ono, A.; Kondo, J. Gold-Mediated Base Pairs in Nucleic Acids: Selective Coordination to Natural and Thiocarbonyl-Modified Cytosines Dependent upon the Oxidation State of Gold. *Chembiochem* **2025**, *26*, e202500565.
(39) Uchiyama, T.; Miura, T.; Takeuchi, H.; Dairaku, T.; Komuro, T.; Kawamura, T.; Kondo, Y.; Benda, L.; Sychrovský, V.; Bouř, P.; et al. Raman spectroscopic detection of the T-Hg^{II}-T base pair and the ionic characteristics of mercury. *Nucleic Acids Res.* **2012**, *40* (12), 5766−5774.
(40) Dairaku, T.; Furuita, K.; Sato, H.; Šebera, J.; Yamanaka, D.; Otaki, H.; Kikkawa, S.; Kondo, Y.; Katahira, R.; Bickelhaupt, F. M.; et al. Direct detection of the mercury-nitrogen bond in the thymine-Hg^{II}-thymine base-pair with ^{199}Hg NMR spectroscopy. *Chem. Commun.* **2015**, *51* (40), 8488−8491.
(41) Dairaku, T.; Furuita, K.; Sato, H.; Šebera, J.; Nakashima, K.; Kondo, J.; Yamanaka, D.; Kondo, Y.; Okamoto, I.; Ono, A.; et al. Structure Determination of an Ag^{I}-Mediated Cytosine-Cytosine Base Pair within DNA Duplex in Solution with ^{1}H/^{15}N/^{109}Ag NMR Spectroscopy. *Chem.—Eur. J.* **2016**, *22* (37), 13028−13031.
(42) Chrisman, R. W.; Mansy, S.; Peresie, H. J.; Ranade, A.; Berg, T. A.; Tobias, R. S. Heavy Metal-Nucleotide Interactions.9. Raman Difference Spectroscopic Studies on Binding of CH_3Hg(II) to 1-Methylthymine, Thymidine-5′-Monophosphate, DNA Models and Native DNA. *Bioinorg Chem.* **1977**, *7* (3), 245−266.
(43) Morzyk-Ociepa, B.; Michalska, D. Vibrational spectra of 1-methylthyminate complexes with mercury(II) and potassium and ab initio calculations of the 1-MeT anion. *J. Mol. Struct.* **2001**, *598* (2−3), 133−144.
(44) Zhang, R. Y.; Pang, D. W.; Zhang, Z. L.; Yan, J. W.; Yao, J. L.; Tian, Z. Q.; Mao, B. W.; Sun, S. G. Investigation of ordered ds-DNA monolayers on gold electrodes. *J. Phys. Chem. B* **2002**, *106* (43), 11233−11239.
(45) Xu, L. J.; Lei, Z. C.; Li, J. X.; Zong, C.; Yang, C. J.; Ren, B. Label-Free Surface-Enhanced Raman Spectroscopy Detection of DNA with Single-Base Sensitivity. *J. Am. Chem. Soc.* **2015**, *137* (15), 5149−5154.
(46) Torigoe, H.; Ono, A.; Kozasa, T. Hg^{II} Ion Specifically Binds with T:T Mismatched Base Pair in Duplex DNA. *Chem.—Eur. J.* **2010**, *16* (44), 13218−13225.
(47) Torigoe, H.; Miyakawa, Y.; Ono, A.; Kozasa, T. Positive cooperativity of the specific binding between Hg ion and T:T mismatched base pairs in duplex DNA. *Thermochim. Acta* **2012**, *532*, 28−35.
(48) Yamaguchi, H.; Šebera, J.; Kondo, J.; Oda, S.; Komuro, T.; Kawamura, T.; Dairaku, T.; Kondo, Y.; Okamoto, I.; Ono, A.; et al. The structure of metallo-DNA with consecutive thymine-Hg^{II}-thymine base pairs explains positive entropy for the metallo base pair formation. *Nucleic Acids Res.* **2014**, *42* (6), 4094−4099.
(49) Šebera, J.; Burda, J.; Straka, M.; Ono, A.; Kojima, C.; Tanaka, Y.; Sychrovský, V. Formation of a Thymine-Hg^{II}-Thymine Metal-Mediated DNA Base Pair: Proposal and Theoretical Calculation of the Reaction Pathway. *Chem.—Eur. J.* **2013**, *19* (30), 9884−9894.
(50) Javornik, U.; Pérez-Romero, A.; López-Chamorro, C.; Smith, R. M.; Dobado, J. A.; Palacios, O.; Bera, M. K.; Nyman, M.; Plavec, J.; Galindo, M. A. Unveiling the solution structure of a DNA duplex with continuous silver-modified Watson-Crick base pairs. *Nat. Commun.* **2024**, *15* (1), 7763.
(51) Genereux, J. C.; Barton, J. K. Mechanisms for DNA Charge Transport. *Chem. Rev.* **2010**, *110* (3), 1642−1662.
(52) Braun, E.; Eichen, Y.; Sivan, U.; Ben-Yoseph, G. DNA-templated assembly and electrode attachment of a conducting silver wire. *Nature* **1998**, *391* (6669), 775−778.

Downloaded from pubs.acs.org/anchem/article-pdf/98/36/26575/6797896/acs.analchem.6c02740.pdf by INST ORGANIC CHEMISTRY AND BIOCHEM user on 23 October 2026

https://doi.org/10.1021/acs.analchem.6c02740
Anal. Chem. 2026, 98, 26575−26582

(53) Porath, D.; Bezryadin, A.; de Vries, S.; Dekker, C. Direct measurement of electrical transport through DNA molecules. *Nature* **2000**, *403* (6770), 635−638.
(54) Kasumov, A. Y.; Kociak, M.; Guéron, S.; Reulet, B.; Volkov, V. T.; Klinov, D. V.; Bouchiat, H. Proximity-induced superconductivity in DNA. *Science* **2001**, *291* (5502), 280−282.
(55) Sebechlebská, T.; Kolivoška, V.; Šebera, J.; Fukal, J.; Řeha, D.; Budešínský, M.; Rosenberg, I.; Bednárová, L.; Gasior, J.; Mészáros, G.; et al. Additive transport in DNA molecular circuits. *J. Mater. Chem. C* **2022**, *10* (33), 12022−12031.
(56) Wang, H. L.; Zhang, Y. K.; Zhang, Z.; Huang, B.; Li, B. L.; Guo, C. L. Base Pair Stacking Modulates Solid-State Charge Transport in DNA Hairpins. *Chem.—Eur. J.* **2023**, *29* (20), e202203540.
(57) Kratochvílová, I.; Vala, M.; Weiter, M.; Spérová, M.; Schneider, B.; Páv, O.; Šebera, J.; Rosenberg, I.; Sychrovský, V. Charge transfer through DNA/DNA duplexes and DNA/RNA hybrids: Complex theoretical and experimental studies. *Biophys Chem.* **2013**, *180*, 127−134.
(58) Benda, L.; Straka, M.; Tanaka, Y.; Sychrovský, V. On the role of mercury in the non-covalent stabilisation of consecutive U-Hg^{II}-U metal-mediated nucleic acid base pairs: metallophilic attraction enters the world of nucleic acids. *Phys. Chem. Chem. Phys.* **2011**, *13* (1), 100−103.
(59) Gruenwedel, D. W. Effect of Hg(II) on the Spectroscopic Properties of DNA Bases - Circular-Dichroism of Deoxyadenosine and Thymidine Monomers and Dimers. *J. Inorg. Biochem* **1994**, *56* (3), 201−212.
(60) Shi, Y. L.; Nakamura, S.; Mitomo, H.; Yonamine, Y.; Wang, G. Q.; Ijiro, K. Plasmonic circular dichroism-based metal ion detection using gold nanorod-DNA complexes. *Chem. Commun.* **2024**, *60* (82), 11794−11797.
(61) Lefringhausen, N.; Seiffert, V.; Erbacher, C.; Karst, U.; Müller, J. Chiral-at-Metal Silver-Mediated Base Pairs: Metal-Centred Chirality versus DNA Helical Chirality. *Chem.—Eur. J.* **2023**, *29* (3), e202202630.
(62) Qu, L.; Zhou, X. M.; Song, J. T.; Zhang, B.; Yang, Q. P.; Zhou, X. G.; Liu, J.; Xiang, H. F. Circularly Polarized Luminescence Switching, Chirality Self-Sorting, and Cell Imaging of Chiral Rhodamine Dyes. *Adv. Opt Mater.* **2023**, *11* (21), 10.1002/adom.202300779.
(63) Polo, A.; Gutiérrez Merino, L.; Rodríguez, R.; Sanz Miguel, P. J. Chirality at Metal in a Linear $[Ag(NHC)_2]^+$ Complex: Stereogenic C-Ag-C Axis, Atropisomerism and Role of $\pi-\pi$ Interactions. *Chem.—Eur. J.* **2024**, *30* (64), e202403239.
(64) Fan, H. H.; Du, C.; Zhang, L.; Liu, M. H. Dual-Mode Amplification of Circularly Polarized Luminescence in DNA Complex Films via Stretching and Photoirradiation. *Acs Mater. Lett.* **2025**, *7* (6), 2125−2132.
(65) Montilla, F.; Carrasco, C. J.; Galindo, A. Chirality in metal-based antimicrobial agents: a growing frontier in biomedical research. *Dalton T* **2025**, *54* (17), 6778−6784.
(66) Adi, W.; Beisenova, A.; Biswas, S. K.; Chen, Y.; Rosas, S.; Unnikrishnan, V.; Zheng, T.; Razeghi Kondelaji, M. H.; Kuruoglu, F.; Arvelo, E. R.; Yesilkoy, F. Unlocking the Translational Potential of Nanophotonic Biosensors: Perspectives on Application-Guided Design. *Acs Photonics* **2025**, *12* (11), 5814−5826.
(67) Vosko, S. H.; Wilk, L.; Nusair, M. Accurate Spin-Dependent Electron Liquid Correlation Energies for Local Spin-Density Calculations - a Critical Analysis. *Can. J. Phys.* **1980**, *58* (8), 1200−1211.
(68) Lee, C. T.; Yang, W. T.; Parr, R. G. Development of the Colle-Salvetti Correlation-Energy Formula into a Functional of the Electron-Density. *Phys. Rev. B* **1988**, *37* (2), 785−789.
(69) Becke, A. D. Density-functional thermochemistry. III. The role of exact exchange. *J. Chem. Phys.* **1993**, *98* (7), 5648−5652.
(70) Stephens, P. J.; Devlin, F. J.; Chabalowski, C. F.; Frisch, M. J. Ab-Initio Calculation of Vibrational Absorption and Circular-Dichroism Spectra Using Density-Functional Force-Fields. *J. Phys. Chem-Us* **1994**, *98* (45), 11623−11627.
(71) Barone, V.; Cossi, M. Quantum calculation of molecular energies and energy gradients in solution by a conductor solvent model. *J. Phys. Chem. A* **1998**, *102* (11), 1995−2001.
(72) Cossi, M.; Rega, N.; Scalmani, G.; Barone, V. Energies, structures, and electronic properties of molecules in solution with the C-PCM solvation model. *J. Comput. Chem.* **2003**, *24* (6), 669−681.
(73) Frisch, M. J. et al. *Gaussian 09, Revision E.01*; Gaussian, Inc.: Wallingford, CT, 2013.
(74) Krishnan, R.; Binkley, J. S.; Seeger, R.; Pople, J. A. Self-Consistent Molecular-Orbital Methods. XX. Basis Set for Correlated Wave-Functions. *J. Chem. Phys.* **1980**, *72* (1), 650−654.
(75) Haussermann, U.; Dolg, M.; Stoll, H.; Preuss, H.; Schwerdtfeger, P.; Pitzer, R. M. Accuracy of Energy-Adjusted Quasi-Relativistic Abinitio Pseudopotentials - All-Electron and Pseudopotential Benchmark Calculations for Hg, HgH and Their Cations. *Mol. Phys.* **1993**, *78* (5), 1211−1224.
(76) Kutzelnigg, W.; Fleischer, U.; Schindler. The IGLO Method: Ab Initio Calculation and Interpretation of NMR Chemical Shifts and Magnetic Susceptibilities. In: *Deuterium and Shift Calculation. NMR - Basis Principles and Progress*, Vol. *23*; Springer: Berlin, Heidelberg, 1990.
(77) London, F. The quantic theory of inter-atomic currents in aromatic combinations. *J. Phys-Paris* **1937**, *8*, 397−409.
(78) Mcweeny, R. Perturbation Theory for Fock-Dirac Density Matrix. *Phys. Rev.* **1962**, *126* (3), 1028−1034.
(79) Ditchfield, R. Self-Consistent Perturbation-Theory of Diamagnetism.1. Gauge-Invariant Lcao Method for Nmr Chemical-Shifts. *Mol. Phys.* **1974**, *27* (4), 789−807.
(80) Wolinski, K.; Hinton, J. F.; Pulay, P. Efficient Implementation of the Gauge-Independent Atomic Orbital Method for Nmr Chemical-Shift Calculations. *J. Am. Chem. Soc.* **1990**, *112* (23), 8251−8260.
(81) Cheeseman, J. R.; Trucks, G. W.; Keith, T. A.; Frisch, M. J. A comparison of models for calculating nuclear magnetic resonance shielding tensors. *J. Chem. Phys.* **1996**, *104* (14), 5497−5509.
(82) Zamora, F.; Sabat, M.; Lippert, B. (1,3-Dimethyluracil-5-yl)mercury(II): Preparative, structural, and NMR spectroscopic studies of an analog of CH_3Hg^{II}. *Inorg. Chem.* **1996**, *35* (17), 4858−4864.
(83) Carmona, P.; Rodríguez-Casado, A.; Molina, M.; Escobar, R. Raman spectroscopic study of uridine nucleotides:: Structural information and conformational features. *J. Raman Spectrosc.* **1999**, *30* (8), 631−636.
(84) Mansy, S.; Tobias, R. S. Heavy Metal-Nucleotide Reactions. IV. Nature of Reaction between Mercury(II) and Uridine or Thymidine - Vibrational Spectroscopic Studies on Binding to N(3), C(4)=O, and C(5) of Uracil Base. *Inorg. Chem.* **1975**, *14* (2), 287−291.
(85) Bouř, P. Computations of the Raman Optical Activity via the sum-over-states expansions. *J. Comput. Chem.* **2001**, *22* (4), 426−435.

Downloaded from pubs.acs.org/anchem/article-pdf/98/36/26575/6797296/acs.analchem.6c02740.pdf by INST ORGANIC CHEMISTRY AND BIOCHEM user on 23 October 2026